Energy Conversion Hot Paper

International Edition: DOI: 10.1002/anie.201509033
German Edition: DOI: 10.1002/ange.201509033

Free-Standing Conducting Polymer Films for High-Performance Energy Devices

Zaifang Li[+], Guoqiang Ma[+], Ru Ge, Fei Qin, Xinyun Dong, Wei Meng, Tiefeng Liu, Jinhui Tong, Fangyuan Jiang, Yifeng Zhou, Ke Li, Xue Min, Kaifu Huo, and Yinhua Zhou**

Abstract: *Thick, uniform, easily processed, highly conductive polymer films are desirable as electrodes for solar cells as well as polymer capacitors. Here, a novel scalable strategy is developed to prepare highly conductive thick poly(3,4-ethylenedioxythiophene):polystyrene sulfonate (HCT-PEDOT:PSS) films with layered structure that display a conductivity of 1400 S cm^{-1} and a low sheet resistance of 0.59 ohm sq^{-1}. Organic solar cells with laminated HCT-PEDOT:PSS exhibit a performance comparable to the reference devices with vacuum-deposited Ag top electrodes. More importantly, the HCT-PEDOT:PSS film delivers a specific capacitance of 120 F g^{-1} at a current density of 0.4 A g^{-1}. All-solid-state flexible symmetric supercapacitors with the HCT-PEDOT:PSS films display a high volumetric energy density of 6.80 mWh cm^{-3} at a power density of 100 mW cm^{-3} and 3.15 mWh cm^{-3} at a very high power density of 16160 mW cm^{-3} that outperforms previous reported solid-state supercapacitors based on PEDOT materials.*

Conducting polymers hold the great advantage of light weight and excellent mechanical flexibility, and have been attracting tremendous attention for the application in electronic devices.[1–4] Among the conducting polymers, poly(3,4-ethylenedioxythiophene (PEDOT)-based materials have been extensively studied because of their excellent air and thermal stability, high transparency in the visible spectral region and tunable conductivity from 10^{-4} to 10^{3} S cm^{-1}.[5–11] The commercially available PEDOT-based aqueous formulation, PEDOT:PSS, has been widely used in organic electronics as the hole-injection or -collection layers, as well as electrodes to replace expensive and brittle indium–tin oxide (ITO) or metals because of the easy processing.[12–16]

Recently, PEDOT-based conducting polymers have also been shown promising as electrodes for flexible supercapacitors.[17,18] D′Arcy et al.[17] reported nanofibrillar PEDOT films prepared by vapor-phase polymerization and the supercapacitors based on the PEDOT electrodes display high specific capacitance and excellent electrochemical stability. Anothumakkool et al.[18] reported a micrometer-thick PEDOT paper obtained by interfacial polymerization. The supercapacitors based on the PEDOT papers show a high specific capacitance of 145 F cm^{-3} and an energy density of 1 mWh cm^{-3}. However, in these reports, the conductivity of the PEDOT nanofibers (130 S cm^{-1})[17] and PEDOT paper (375 S cm^{-1})[18] are lower than that of optimized thin (less than 100 nm) PEDOT-based films (over 1000 S cm^{-1}) processed from commercially available PEDOT:PSS formulations PH1000 with post-treatment.[19,20] The potentially higher conductivity could possibly further enhance the performance of the supercapacitors. However, it has been a challenge to prepare thick, uniform, highly conductive PEDOT-based films from the commercially available formulations because of the limit of the concentration.

Herein, we report a novel strategy to prepare a uniform, highly conductive, thick PEDOT:PSS film (HCT-PEDOT:PSS) from commercially available PEDOT:PSS formulations for energy conversion and storage devices. The preparation procedures are shown schematically in Figure 1 a and the actual pictures of each procedure are shown in Figure S1 in the Supporting Information. The key point of this strategy to prepare the HCT-PEDOT:PSS film is that the binding between PEDOT and PSS can be broken by sulfuric acid as shown in Equation (S1). The PEDOT:PSS aqueous dispersion forms disk-shaped precipitates when dropped into a dilute sulfuric acid solution because of the removal of the outer-ring PSS (that acts as a dispersion agent) in the PEDOT:PSS drop (Figure 1 a). Then the precipitate is turned into PEDOT:PSS paste by stirring and cast onto a filter paper. It should be mentioned that the PEDOT:PSS paste does not go through the filter paper while the commercially available PH1000 formulation can easily transmit the paper (Figure S2). The filter paper is next dissolved by immersing into acetone. The free-standing films are immersed into a concentrated sulfuric acid to achieve a high conductivity.[19,20]

Figure 1 b shows a picture of the free-standing HCT-PEDOT:PSS film and the cross-sectional SEM image of a free-standing HCT-PEDOT:PSS film. Layered structure can be observed from the SEM image. The film thickness is about 2.78 μm. The sheet resistance of film is 2.60 Ω sq^{-1} and the conductivity is about 1400 S cm^{-1}. The sheet resistance is further reduced to 0.59 Ω sq^{-1} when the HCT-PEDOT:PSS film is 16-μm thick. The HCT-PEDOT:PSS film could also be paved onto substrates (such as PES, PET, glass, and so forth) besides the free-standing ones. Figure S3 shows photographs

[*] Dr. Z. F. Li,[+] G. Q. Ma,[+] R. Ge, F. Qin, X. Y. Dong, W. Meng, T. F. Liu, J. H. Tong, F. Y. Jiang, Y. F. Zhou, K. Li, X. Min, Prof. Dr. K. F. Huo, Prof. Dr. Y. H. Zhou
Wuhan National Laboratory for Optoelectronics and School of Optical and Electronic Information
Huazhong University of Science and Technology
Wuhan 430074 (China)
E-mail: kfhuo@hust.edu.cn
yh_zhou@hust.edu.cn

[+] These authors contributed equally to this work.

Supporting information for this article is available on the WWW under http://dx.doi.org/10.1002/anie.201509033.

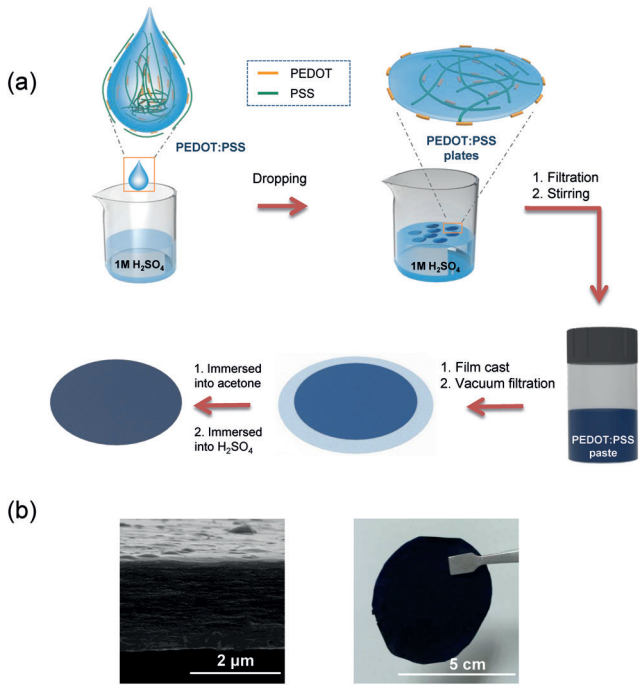

Figure 1. a) Schematic illustrations for the fabrication procedure of a HCT-PEDOT:PSS film. First, PH1000 was dropwise added into a dilute H_2SO_4 solution to obtain PEDOT:PSS plates. Then the PEDOT:PSS plates was turned into a paste by high-speed stirring. The paste was then cast onto a filter paper and the filtrate was separated by a vacuum filtration. The film was then immersed in acetone and thereafter immersed into a concentrated H_2SO_4 solution to achieve high-conductivity HCT-PEDOT:PSS films. b) Image of the free-standing HCT-PEDOT:PSS film. Cross-sectional SEM image of the HCT-PEDOT:PSS film.

of HCT-PEDOT:PSS films on a glass substrate and a poly(-ether sulfonate) (PES) substrate.

To further understand the structure characteristics of the HCT-PEDOT:PSS film, XPS and XRD measurements were carried out on the HCT-PEDOT:PSS samples. Figure S4a–c shows the XPS spectra of the different films, from which we can estimate that the PSS ratios were reduced from 73.8% (PH1000) to 11.9% (HCT-PEDOT:PSS). The removal of PSS is beneficial to the conductivity and air stability and could also reduce the causticity. The films before final sulfuric acid treatment (denoted as 1MS-PEDOT:PSS) are also characterized by XPS as shown in Figure S4b. The PSS ratio is calculate to be 70.6%. The conductivity of the 1MS-PEDOT film is about 340 $S\,cm^{-1}$. Figure S5a presents the XRD patterns of the two different films. For the HCT-PEDOT:PSS films, the peak intensity at around 6.0° and 12.0° significantly increases which indicates an increased lamella stacking and improved crystallinity in the HCT-PEDOT:PSS films. This result is well consistent with the enhanced conductivity. The conductivity of the film was kept almost constant after being left in air for over six months.

The HCT-PEDOT:PSS film has a high work function of 5.13 ± 0.01 eV measured by scanning Kelvin probe. The free-standing HCT-PEDOT:PSS films were laminated as the top electrode for hole collection in organic solar cells with an inverted structure of glass/ITO/PEI/P3HT:ICBA/PEDOT:PSS (4083)/HCT-PEDOT:PSS (Figure S6a; PEI = polyethylenimine, P3HT = poly(3-hexylthiophene-2,5-diyl), and ICBA = indene–C60 bisadduct). The device with an effective area of 5 mm^2 exhibits an excellent performance of $V_{OC} = 0.81$ V, $J_{SC} = 8.65\,mA\,cm^{-2}$, FF = 66%, and PCE = 4.6% (Figure S6b). We further fabricated organic solar cells with a larger area of 66 mm^2 since the electrode has a low sheet resistance. The device also displays good performance of $V_{OC} = 0.80$ V, $J_{SC} = 8.26\,mA\,cm^{-2}$, FF = 62%, and PCE = 4.1%. As a reference, an inverted organic solar cell with vacuum-deposited Ag as the top electrodes was also fabricated (Figure S7a) and the *J*–*V* characteristics are shown in Figure S7b. This device (5 mm^2) demonstrates a PCE of 4.5% similar to that of HCT-PEDOT:PSS electrode-based solar cells. These results show that the HCT-PEDOT:PSS films are competent as the top electrode for organic solar cells with potentially low-cost vacuum-free processing.

The electrochemical performance of the HCT-PEDOT:PSS film (2.78 μm) was investigated by cyclic voltammetry (CV) and a galvanostatic charge–discharge (GCD) test in a three-electrode configuration. The cyclic voltammograms (Figure 2a) display rectangular characteristics, indicating their excellent capacitive properties. The GCD curves are shown in Figure 2b in a voltage window of −0.2–0.8 V. The GCD curves still remain a triangular shape even at a very large current density of 20 $A\,g^{-1}$ which further confirms the excellent capacitive properties of the HCT-PEDOT:PSS electrodes. Figure 2c shows the specific capacitances under different current densities. It can be seen that

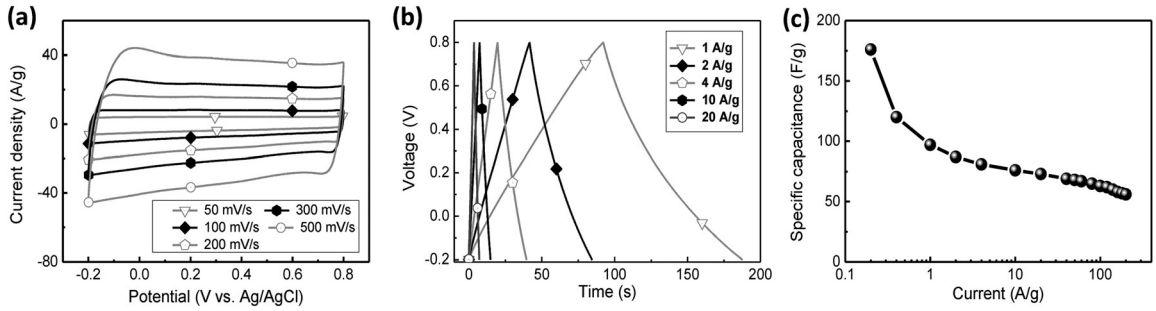

Figure 2. a) Cyclic voltammograms of HCT-PEDOT:PSS films recorded at different scan rate of 50, 100, 200, 300, and 500 $mV\,s^{-1}$. b) Charge–discharge profiles of HCT-PEDOT:PSS films recorded at different current density of 1, 2, 4, 10, 20 $A\,g^{-1}$. c) The specific capacitance as a function of current density.

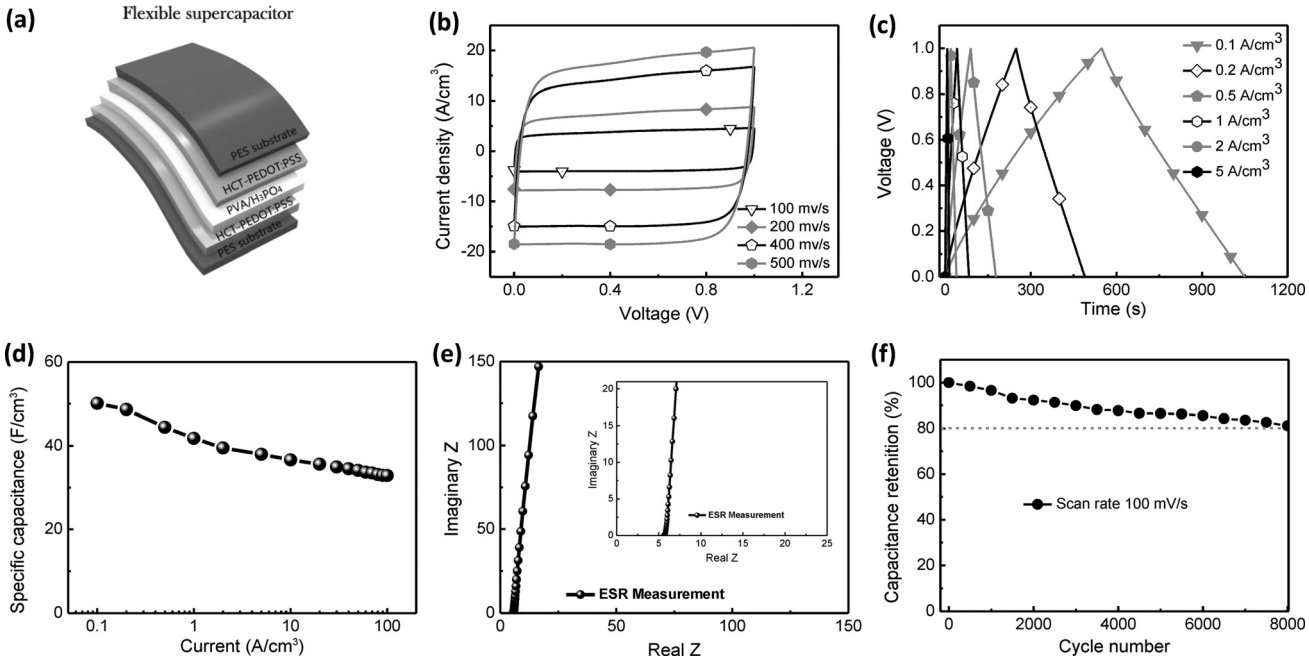

Figure 3. a) Structure of solid-state flexible supercapapcitors. b) CV curves of the supercapacitors recorded at different scan rates of 100, 200, 400, and 500 $mV s^{-1}$. c) CD profiles of the supercapacitors recorded at different current density of 0.1, 0.2, 0.5, 1, 2, and 5 $A cm^{-3}$. d) Specific capacitance as a function of current density. e) Nyquist plots of the flexible solid-state device with an enlarged photograph in the inset. f) Cycling stability of the solid-state flexible supercapacitor with a relatively high scan rate of 100 $mV s^{-1}$.

a high specific capacitance of 176 $F g^{-1}$ is achieved at a current density of 0.2 $A g^{-1}$.

Because of its high conductivity and flexible properties, the HCT-PEDOT:PSS film is used to construct flexible all-solid-state supercapacitors (Figure 3a). Electrochemical charge–storage properties were measured using CV, GCD tests, and electrochemical impedance spectroscopy (EIS). Figure 3b shows the CV characteristics of HCT-PEDOT:PSS-based flexible all-solid-state supercapacitors. The rectangle shape of the CV curves indicates that devices based on HCT-PEDOT:PSS possess excellent electrical conductivity. Figure 3c displays the GCD profiles of flexible supercapacitors based on HCT-PEDOT:PSS electrodes. The volumetric capacitance is calculated to be 50.1 $F cm^{-3}$ at a current density of 0.1 $A cm^{-3}$ (Figure 3d). What is exciting is that a high volumetric capacitance of 32.9 $F cm^{-3}$ could be obtained even at an extremely high current density of 100 $A cm^{-3}$. The density of HCT-PEDOT:PSS is estimated to be about 1 $g cm^{-3}$. The corresponding specific capacitance with a current density of 0.1 $A cm^{-3}$ is about 50.1 $F g^{-1}$ while the specific capacitance with a large current density of 100 $A cm^{-3}$ is about 32.9 $F g^{-1}$. The high conductivity and the layered structure of HCT-PEDOT:PSS films could possibly be the reason of devices retaining high capacitance under high current density.

The highly conductive property of the HCT-PEDOT:PSS electrodes was further proved by electrochemical series resistance (ESR) measured using EIS, which demonstrates an extremely low resistance of 5.7 Ω (Figure 3e) and this value is well consistent with that of HCT-PEDOT:PSS film sheet resistance. A long-term cycle stability test was performed at a high scan rate of 100 $mV s^{-1}$ for 8000 cycles and over 80% of the specific capacitance is retained, suggesting excellent cycle stability (Figure 3f). The initial reduced capacitance should be attributed to the loss of water from the PVA/H_3PO_4 gel electrolyte resulting from the generated heat during the cycles.

Energy density and power density of the flexible devices were key parameters for practical applications of the supercapacitors. Figure 4a shows the Ragone plot of devices. A maximum energy density of 6.95 $mW h cm^{-3}$ was obtained with a power density of 50 $mW cm^{-3}$. It is surprising that devices could maintain an energy density of 3.54 $mW h cm^{-3}$ at a high power density of 12815 $mW cm^{-3}$ and 3.15 $mW h cm^{-3}$ at a power density of 16160 $mW cm^{-3}$. For comparison, values of two recently published articles[17,18] are also plotted in Figure 4a, from which we can find that our devices display a much higher energy density and power density. The mechanical stability of the device under various conditions of bending (angles of 30°, 60°, and 90°) and twisting (Figure 4b) was also investigated and found to be high according to a series of CV tests at a scan rate of 100 $mV s^{-1}$. From the CV curves we can find that the solid-state flexible device maintains a very stable performance under the conditions of bending and twisting. The solid-state flexible supercapacitors connected in series and parallel are also demonstrated. Figure 4c shows the GCD profiles of two solid-state flexible supercapacitors of devices A and B with identical device structure as shown in Figure 3a and the two devices in parallel and series connections at a current density of 0.5 $A cm^{-3}$. It can be observed that the devices in both series and parallel could double the performance. All above results demonstrate that the HCT-PEDOT:PSS film is a good candidate as an efficient flexible electrode for the supercapacitors.

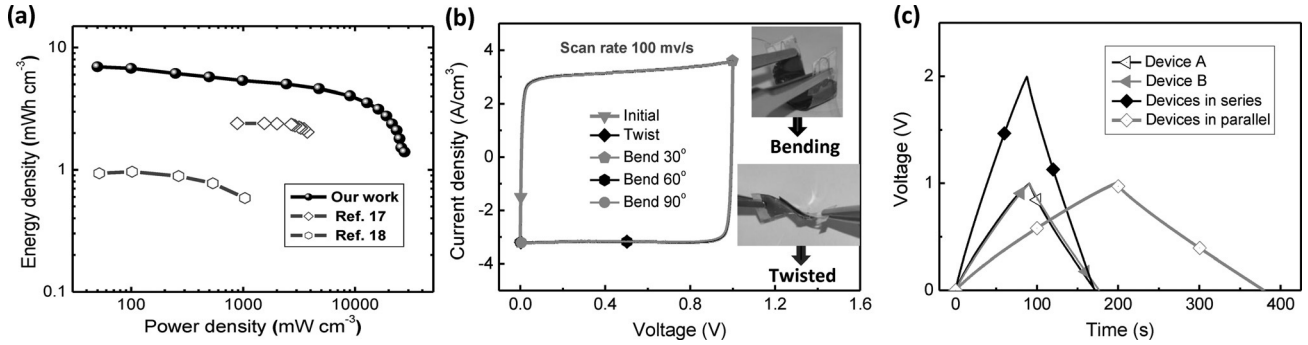

Figure 4. a) Energy density and power density Ragone plots of the flexible solid-state supercapacitors comparing our work and the state-of-the-art reports of PEDOT-based supercapacitors in the literature. b) Cyclic voltammograms of the flexible solid-state supercapacitor under different bending angles (30°, 60°, 90°) and twisting conditions. c) CD profiles of solid-state flexible device supercapacitors of unconnected and in series and in parallel connected devices A and B at a current density of 0.5 A cm^{-3}.

In summary, we have developed a novel strategy to fabricate micrometer-thick, highly conductive, free-standing PEDOT:PSS films processed from commercially available aqueous dispersions. The films display a high conductivity of 1400 S cm^{-1}, which is the highest conductivity reported in a micrometer-thick conducting polymer films. The films exhibit good air stability and flexibility. Furthermore, the films are easily scaled up to large areas by the reported technique. We have also reported that the flexible free-standing films were successfully laminated as the top electrode for vacuum-free organic solar cells. More importantly, flexible solid-state supercapacitors based on the polymer electrodes display an energy density of 3.15 mWh cm^{-3} at a very high power density of 16160 mW cm^{-3} that outperforms previously reported PEDOT-based supercapacitors. The supercapacitors also exhibit good electrochemical charge–discharge cycling stability and flexibility. Beside the demonstrated solar cells and supercapacitors, we believe the films can be used potentially for many other applications, such as thermoelectric applications or batteries.

Acknowledgements

The work is supported by the Recruitment Program of Global Youth Experts, the National Natural Science Foundation of China (grant number 21474035), the Fundamental Research Funds for the Central Universities, HUST (grant number 2014YQ013), Postdoctoral Science Foundation of China (grant numbers 2014M562016 and 2015T80794).

Keywords: conducting polymers · energy conversion · polymer electrodes · solar cells · supercapacitors

How to cite: *Angew. Chem. Int. Ed.* **2016**, *55*, 979–982
Angew. Chem. **2016**, *128*, 991–994

[1] O. Bubnova, Z. U. Khan, A. Malti, S. Braun, M. Fahlman, M. Berggren, X. Crispin, *Nat. Mater.* **2011**, *10*, 429–433.
[2] G. H. Kim, L. Shao, K. Zhang, K. P. Pipe, *Nat. Mater.* **2013**, *12*, 719–723.
[3] J. E. Yoo, K. S. Lee, A. Garcia, J. Tarver, E. D. Gomez, K. Baldwin, Y. Sun, H. Meng, T.-Q. Nguyen, Y.-L. Loo, *Proc. Natl. Acad. Sci. USA* **2010**, *107*, 5712–5717.
[4] N. K. Unsworth, I. Hancox, C. Argent Dearden, P. Sullivan, M. Walker, R. S. Lilley, J. Sharp, T. S. Jones, *Org. Electron.* **2014**, *15*, 2624–2631.
[5] N. Kim, B. H. Lee, D. Choi, G. Kim, H. Kim, J.-R. Kim, J. Lee, Y. H. Kahng, K. Lee, *Phys. Rev. Lett.* **2012**, *109*, 106405.
[6] W. Meng, R. Ge, Z. Li, J. Tong, T. Liu, Q. Zhao, S. Xiong, F. Jiang, L. Mao, Y. Zhou, *ACS Appl. Mater. Interfaces* **2015**, *7*, 14089–14094.
[7] K. van de Ruit, R. I. Cohen, D. Bollen, T. van Mol, R. Yerushalmi-Rozen, R. A. J. Janssen, M. Kemerink, *Adv. Funct. Mater.* **2013**, *23*, 5778–5786.
[8] X. Hu, L. Chen, Y. Zhang, Q. Hu, J. Yang, Y. Chen, *Chem. Mater.* **2014**, *26*, 6293–6302.
[9] Q. Wei, M. Mukaida, Y. Naitoh, T. Ishida, *Adv. Mater.* **2013**, *25*, 2831–2836.
[10] J. Ouyang, *Displays* **2013**, *34*, 423–436.
[11] A. I. Hofmann, W. T. T. Smaal, M. Mumtaz, D. Katsigiannopoulos, C. Brochon, F. Schîtze, O. R. Hild, E. Cloutet, G. Hadziioannou, *Angew. Chem. Int. Ed.* **2015**, *54*, 8506–8510; *Angew. Chem.* **2015**, *127*, 8626–8630.
[12] Y. H. Zhou, F. H. Li, S. Barrau, W. J. Tian, O. Inganas, F. L. Zhang, *Sol. Energy Mater. Sol. Cells* **2009**, *93*, 497–500.
[13] Y. H. Zhou, C. Fuentes-Hernandez, J. Shim, J. Meyer, A. J. Giordano, H. Li, P. Winget, T. Papadopoulos, H. Cheun, J. Kim, M. Fenoll, A. Dindar, W. Haske, E. Najafabadi, T. M. Khan, H. Sojoudi, S. Barlow, S. Graham, J. L. Bredas, S. R. Marder, A. Kahn, B. Kippelen, *Science* **2012**, *336*, 327–332.
[14] S.-I. Na, S.-S. Kim, J. Jo, D.-Y. Kim, *Adv. Mater.* **2008**, *20*, 4061–4067.
[15] F. L. Zhang, M. Johansson, M. R. Andersson, J. C. Hummelen, O. Inganas, *Adv. Mater.* **2002**, *14*, 662–665.
[16] T. T. Larsen-Olsen, R. R. Sondergaard, K. Norrman, M. Jorgensen, F. C. Krebs, *Energy Environ. Sci.* **2012**, *5*, 9467–9471.
[17] J. M. D'Arcy, M. F. El-Kady, P. P. Khine, L. Zhang, S. H. Lee, N. R. Davis, D. S. Liu, M. T. Yeung, S. Y. Kim, C. L. Turner, A. T. Lech, P. T. Hammond, R. B. Kaner, *ACS Nano* **2014**, *8*, 1500–1510.
[18] B. Anothumakkool, R. Soni, S. N. Bhange, S. Kurungot, *Energy Environ. Sci.* **2015**, *8*, 1339–1347.
[19] Y. Xia, K. Sun, J. Ouyang, *Adv. Mater.* **2012**, *24*, 2436–2440.
[20] N. Kim, S. Kee, S. H. Lee, B. H. Lee, Y. H. Kahng, Y. R. Jo, B. J. Kim, K. Lee, *Adv. Mater.* **2014**, *26*, 2268–2272.

Received: September 26, 2015
Revised: November 9, 2015
Published online: December 2, 2015

